High-pressure magnetic properties of antiferromagnetic samarium up to 30 GPa using a SQUID-based vibrating coil magnetometer

Masaki Mito,[1,*] Hirotaka Kondo,[1] Taiki Arase,[1] Kunihiko Irie,[1] Seishi Takagi,[1] Hiroyuki Deguchi,[1] Takayuki Tajiri,[2] and Mamoru Ishizuka[3]

[1]*Graduate School of Engineering, Kyushu Institute of Technology, Kitakyushu 804-8550, Japan*

[2]*Faculty of Science, Fukuoka University, Fukuoka 814-0180, Japan*

[3]*Center for Scientific Instrument Renovation and Manufacturing Support, Osaka University, Toyonaka 560-0043, Japan*

(Received 18 February 2021; revised 17 July 2021; accepted 2 August 2021; published 23 August 2021)

Samarium (Sm) has antiferromagnetic (AFM) ordering at the hexagonal site at $T_N(\text{hex}) = 106$ K, and at the cubic site at $T_N(\text{cub}) = 14$ K at ambient pressure. The structural transition from the so-called Sm-type structure to the double hexagonal close-packed (dhcp) structure occurs at approximately 6 GPa. According to electrical resistance measurements, the shift of $T_N(\text{hex})$ toward the low-temperature side occurs simultaneously with the shifting of $T_N(\text{cub})$ toward the high-temperature side with increasing pressure. We conducted dc magnetic measurements on Sm at high pressure up to 30 GPa using a SQUID-based vibrating-coil-magnetometer to pursue $T_N(\text{cub})$ at high pressure: The magnetic measurements revealed stepwise anomalies below 2 GPa. A ferromagnetic (FM) anomaly was observed in the dhcp structure, suggesting that spins at both structural sites formed the FM magnetization. In the face-centered cubic (fcc) structure at above 12 GPa, a reduction in the magnetic signal occurred. In the distorted fcc structure at above 20 GPa, sufficient suppression of the FM moment was observed and afterward the diamagnetic signal suggesting the possibility of superconductivity was observed.

DOI: 10.1103/PhysRevB.104.054431

I. INTRODUCTION

In the periodic table, samarium (Sm) is an element with antiferromagnetic (AFM) properties. Europium (Eu), located on the right side of Sm, becomes a superconductor at a pressure (P) of above 80 GPa [1]. Six lanthanide elements from gadolinium (Gd) to thulium (Tm) on the right side of Eu are ferromagnetic (FM) elements. Among the lanthanide metals, the exchange interaction between localized moments of f-orbital electrons via the conduction electrons is called the Ruderman-Kittel-Kasuya-Yosida (RKKY) interaction [2–4]. Five FM elements, except for Gd, have an incommensurate antiferromagnetic phase at the high-temperature side of the FM phase. Thus, there are various magnetic and electronic properties in the element groups from Sm to Tm. The trivalent lanthanide elements exhibit structural phase transition sequences, such as hexagonal close-packed (hcp) → Sm-type → double hcp (dhcp) → face-centered cubic (fcc) → distorted-fcc (dfcc) with increasing P [5,6]. The FM state for Gd-holmium (Ho) stably exists in the hcp structure prior to the Sm-type one [7]. It is quite important to know the magnetic properties of Sm at various P values.

The crystal structure of Sm undergoes successive structural transitions at the following pressures: Sm-type → dhcp at 6 GPa, dhcp → fcc at 13–15 GPa, and fcc → dfcc at 20 GPa [5]. In 1972, the neutron scattering of single crystals of Sm revealed two kinds of AFM ordering at the Néel temperatures $T_N(\text{hex}) = 106$ and $T_N(\text{cub}) = 13.8$ K, which are related to the AFM ordering of the moments at the hexagonal and cubic sites, respectively [8]. The first ordering was also confirmed by x-ray diffraction in 1993 [9]. Before 1972, for arc-melted or distilled Sm, anomalies in electrical resistivity [10], magnetic susceptibility [10], and specific heat [11] had already been observed at these temperatures. On the other hand, Sm is also an interesting element from the viewpoint of valence fluctuations between divalent and trivalent states [12], and it is well known that the valence of Sm compounds often changes with pressures [13]. With regard to high-pressure experiments on Sm, changes in the Néel temperatures $T_N(\text{hex})$ and $T_N(\text{cub})$ were determined by electrical resistance (R) measurements [14–16]. The temperature (T) derivative dR/dT became essential to identifying anomalies at high pressure because the temperature dependence of R became more gradual with increasing pressure. According to the R measurements, the shift of $T_N(\text{hex})$ toward the low-temperature side, occurred simultaneously with the shifting of $T_N(\text{cub})$ toward the high-temperature side with increasing P. Regardless of its long history, magnetic measurements of Sm have not been conducted owing to the small AFM signals per unit volume.

Given the previous studies on terbium, dysprosium, and Ho, the electrical resistance is insufficient to pursue two kinds of magnetic orderings correlated with conduction electrons. Recently, the importance of precise magnetization measurements at high pressure using a superconducting quantum interference device (SQUID) was verified in the high-pressure experiment for Gd-Ho [7,17]. The magnetic phase diagram of Sm based on R-T measurements must also be confirmed by magnetic measurements. In the present study, we conducted dc magnetic susceptibility measurements on Sm using

*mitoh@mns.kyutech.ac.jp

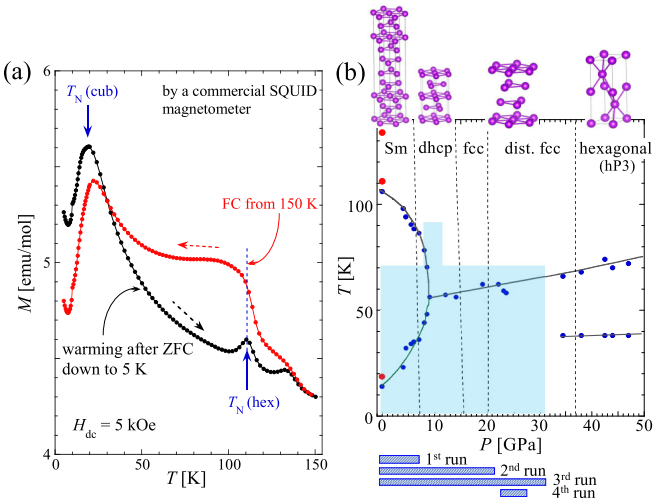

FIG. 1. (a) T-dependence of magnetization M of 186.6-mg polycrystalline Sm composed of many fragments with a rectangular shape of approximately 0.5 mm × 0.5 mm at $H_{dc} = 5$ kOe and ambient pressure, measured using a commercial SQUID magnetometer. The measurement was performed in the warming process to 150 K after ZFC and the following FC process. (b) P-T phase diagram for Sm based on previous electrical resistance measurements [15]. The red circles present Ts with magnetic anomaly at $H_{dc} = 5$ kOe, shown in (a). The P-T region covered in the present experiment is shaded in light blue. The P range of four runs is shown by the blue bars.

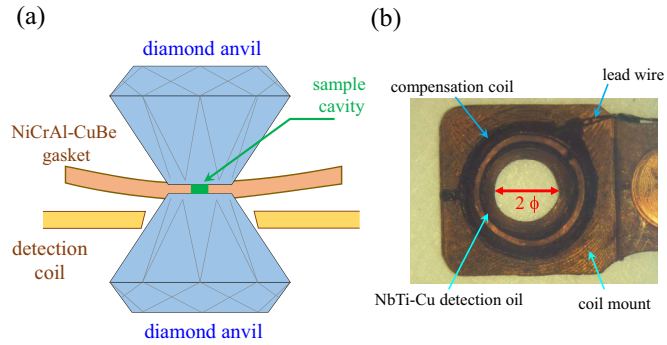

FIG. 2. (a) Overview of the setup of SQUID-VCM: The use of diamond anvils with different culet size (i.e., 500 and 550 μm) allows the CuBe-NiCrAl composite gasket to be deformed away from the detection coil. (b) Picture of the detection coil made of NbTi wire (30-μm diameter) coated with Cu. The diameter of the wire, including the Cu and insulating layers, is 50 μm. The 20-turn detection coil was prepared around the bore with a diameter of 2 mm; the outside has a 10-turn compensation coil.

a vibrating-coil SQUID magnetometer, which provided a sensitive magnetic measurement for extremely small samples in a diamond anvil cell (DAC) because the location of the detection coil vibrating slightly above the gasket is near the maximum point of the gradient of the magnetic flux due to the sample magnetization.

II. EXPERIMENTAL METHODS

In the present experiment, a polycrystalline sample of Sm with a purity of 99.9% (Nippon Yttrium Co., Ltd.) was used. Small specimens with a rectangular shape of approximately 50 μm × 50 μm and the thickness of approximately 10 μm were selected for the high-pressure experiments. They have structural orientation according to the x-ray diffraction analysis. This high purity was also verified by the energy dispersive x-ray spectroscopy, where no metallic elements except for Sm were observed. For the sake of the sample check, we also performed the magnetization M measurement using many fragments with a rectangular shape of approximately 0.5 mm × 0.5 mm at the dc magnetic field $H_{dc} = 5$ kOe in the warming process to 150 K after zero-field cooling (ZFC) and the following field cooling (FC) process using a commercial SQUID magnetometer. In Fig. 1(a), the data on M of the 186.6-mg polycrystalline Sm composed of many fragments at $H_{dc} = 5$ kOe as a function of T show one anomaly observed at 18 K and two anomalies at above 100 K (110 K and 134 K). The M in the FC process rapidly increases at approximately 115 K, and the T dependence of M below 115 K seems to be ferromagnetic at first glance. Similar behavior was also confirmed in another sample that was a powder sample with a purity of 99.9 % (NewMet Ltd.). According to the literature of Ref. [8], the anomalies at 18 K and 110 K correspond to the magnetic ordering at T_N(cub) and T_N(hex), respectively.

The melting point for Sm is 1345 K. Generally, it is mechanically known that the residual strain is usually released by being annealed at T more than a half of melting point. In the polycrystals annealed at 851 K for 1.5 hours, the magnetic anomaly at 134 K was reduced down to one-tenth of that at 110 K, suggesting the anomaly at 134 K might be due to a short-ranged ordering at the hexagonal sites. Indeed, the anomaly at 134 K was not observed in the pretty old study using the Sm specimens obtained from the arc-melted ingot [10]. However, M of the above polycrystals annealed at 851 K became ten times larger than that for nonstrained sample. Further, the anomaly at T_N(hex) was larger than that at T_N(cub) not consistently with the result for the arc-melted specimen [10], so that we used the nonannealed polycrystals in the present magnetic measurements. The magnetic measurements for Sm via four runs covered the hatched region with light blue in the P-T phase diagram in Fig. 1(b), and herein we are principally going to pursue the P dependence of T_N(cub).

A DAC was mounted at the bottom of a 1K pot in a ^{4}He refrigerator. The use of diamond anvils (Type-I, 2.4-mm height) with different culet sizes (i.e., 500 and 550 μm) led to the deformation of the CuBe-NiCrAl composite gasket away from the NbTi detection coil as seen in Fig. 2(a). The NiCrAl disk with a diameter of 410 μm was inserted into the hole drilled at the center of the CuBe gasket [18]. After pressing the composite gasket with the initial thickness of 250 μm down to approximately 130 μm, a hole with a diameter of 200 μm was drilled at the center. As already seen in the data at $P = 30$ GPa in Ref. [19], we also confirmed that, in another experiment focusing 29–33 GPa, the presnet system using the CuBe-NiCrAl gasket does not show any characteristic anomaly below 60 K. In the sample cavity, some polycrystalline pieces of Sm were held together by the pressure-transmitting medium Daphne 7373 [20], with ruby as the manometer at room temperature, and lead as the manometer at liquid ^{4}He temperature. The magnitude of P was estimated at room temperature by mea-

suring the fluorescence of the ruby [21], whereas the P value at liquid ^{4}He temperature was at most 1.1 times of that at room temperature. The coil composed with inner detection and outer compensation consisted of NbTi wires covered with Cu as shown in Fig. 2(b). By strengthening the cooling contact between the NbTi coil and the 1-K pot with Cu coating, the maximum T for transforming the magnetic flux to a voltage using the SQUID was increased from 70–80 K to 115 K.

The vibration frequency of the detection coil was chosen to be 168 Hz near the resonating frequency of the piezoelectric actuator of bimorph type. The detection coil was vibrated with an amplitude of 10 micron along the directions of both the anvil axis and H_{dc}, and it was decoupled thermally from the gasket containing sample and the body of DAC. The output voltage from the SQUID-based vibrating-coil-magnetometer (VCM), V_{VCM}, was increased along with H_{dc}. The maximum H_{dc} was 110 Oe. For FM signals, the FC process can enhance V_{VCM} [19,22]. The change in magnetic ordering temperatures at high pressure will be evaluated via the P-T phase diagram including the V_{VCM} intensity.

III. EXPERIMENTAL RESULTS

A. T-dependence of V_{VCM} over Sm-tyre, dhcp, fcc, and distorted fcc structures

Figures 3(a) to 3(c) show the T-dependence of V_{VCM} for Sm in the first run at $H_{dc} = 30$ Oe. As shown in Fig. 3(a), at $P = 0$ GPa, V_{VCM} in the warming process after ZFC decreased at 15–21 K because of the collapse of the AFM ordering at the cubic sites. The characteristic T values were denoted as #1 and #2 (#2 will be connected with the anomalies in R above 35 GPa [15] [see Fig. 1(b)]. They varied in the FC process, with a slight change between the FC process and warming process after FC. In the warming process to a higher T after FC, new characteristic Ts, denoted as #3 and #4, were observed, which indicated a series of stepwise behaviors. Thus, at $P = 0$ GPa, the unique magnetic property at small H_{dc} is not stable against the change in T. When T_N(cub) $< T <$ T_N(hex), ordered and disordered spins coexist, and glassy behavior appears. Figure 3(b) shows that at 2.0 GPa, the magnetic anomalies observed after FC hardly shifted compared with those at 0 GPa, whereas the intensity of V_{VCM} increased. Because of unintentional mistakes in sample preparation, pieces of the manometer Pb were placed both inside and outside the cavity of the gasket, and the first superconducting signal shifted toward the lower T side. The superconducting signal of Pb, located at the side of Sm, appeared on the side of positive magnetization, unlike that at $P = 0$ GPa. This behavior was observed in the experiment on a ferromagnet accompanied by the enhancement of magnetization at pressures [22]. Strictly speaking, the occurrence of phenomenon depends on the delicate positioning of Pb against a ferromagnetic sample (in the Supplemental Material, the detailed explanation is presented using Fig. S1 [23]). The present behavior suggests that the magnetization of Sm is enhanced by initial pressurization from 0 → 2.0 GPa. As seen in Fig. 3(c), further pressurization to 5.9 GPa enhanced the magnetization by up to 10 times that at $P = 0$ GPa. A stepwise behavior was fairly suppressed there. The T-dependence of V_{VCM} changed to a typical FM style, and the difference

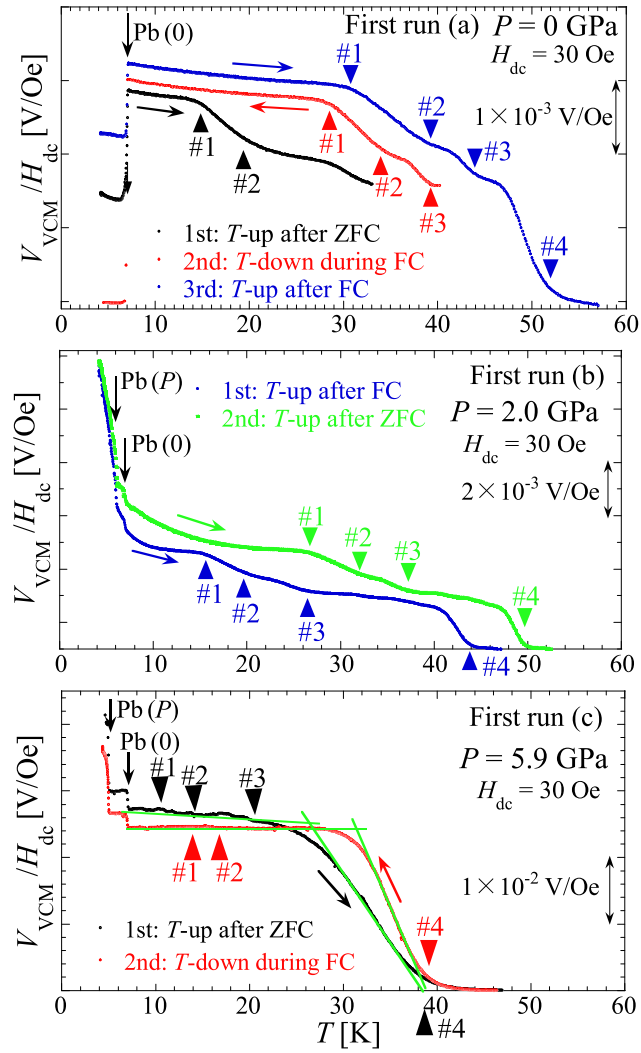

FIG. 3. T-dependence of V_{VCM} for the first run. V_{VCM} proportional to the magnetization is normalized with the dc magnetic field H_{dc}, resulting in a relative dc magnetic susceptibility. The first run covers a pressure range of up to 6 GPa (near the border between the Sm-type and dhcp structures [(a) 0, (b) 2.0, and (c) 5.9 GPa]. A series of magnetic anomalies for Sm is presented with closed triangles.

between ZFC and FC became very small, leading to the easy evaluation of the Curie temperature of 40 K. Sm originally has an AFM correlation and two structural sites. The above FM behavior surely originates from a ferrimagnetic or weak-FM state.

The change in the T-dependence of V_{VCM} at $P > 6$ GPa was confirmed in the second run [see Fig. 4(a)], where the intensity of V_{VCM} reached a maximum at $P = 8.3$ GPa. The Curie temperature at $P = 8.3$ and 12.8 GPa was over 50 K. At $P = 20.5$ GPa in the fcc phase, the FM signal was almost suppressed. As seen in Fig. 4(b), at $P = 23.1$ GPa in the distorted fcc phase, a diamagnetic signal, not due to Pb, appeared at approximately 6 K. The aforementioned phenomenon will be observed in the third and fourth runs.

Figures 5 and 6 show the T-dependence of V_{VCM} for the third run, covering the P range to 30.8 GPa. The data in the warming process after FC are presented. The data for

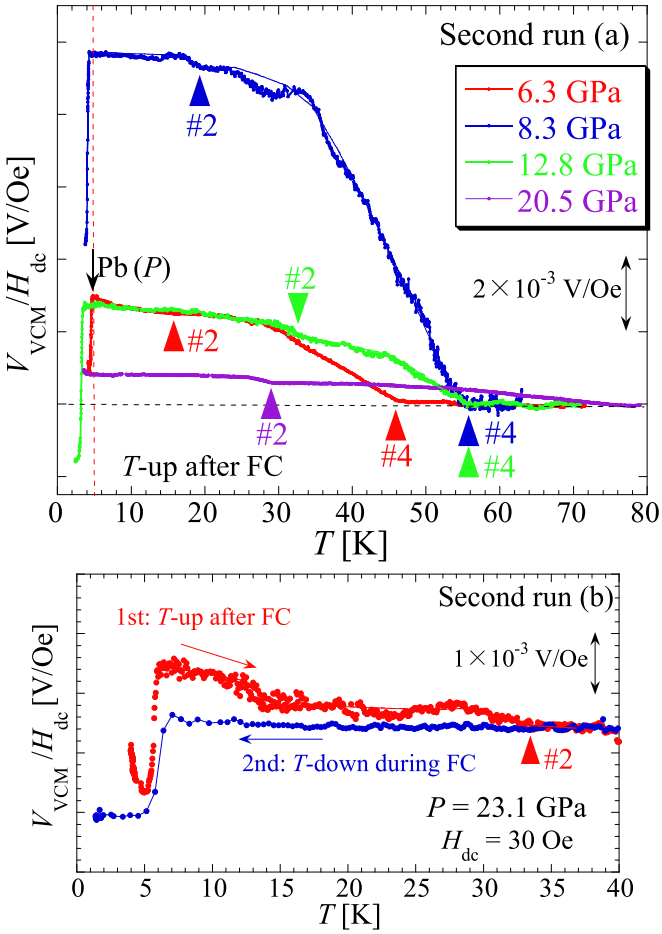

FIG. 4. T-dependence of V_{VCM} for Sm in the second run. V_{VCM} proportional to the magnetization is normalized with the applied dc magnetic field H_{dc}. In the second run, the pressure range increased to 23.1 GPa, below which the structure changed from Sm-type → dhcp → fcc → distorted fcc structures: [(a) 6.3–20.5 GPa and (b) 23.1GPa]. The H_{dc} in (a) is 17 Oe at 6.3 GPa, 13 Oe at 8.3 and 12.8 GPa, and 10 Oe at 20.5 GPa. In (a), the T position of the diamagnetic signal of Pb at $P = 6.3$ GPa is marked with a red broken line and a black arrow. A series of magnetic anomalies for Sm is marked with closed triangles.

$P \leqslant 21.1$ GPa in the wide T range are presented in Fig. 5. The stepwise $V_{VCM}(T)$ at 0 GPa is similar to that in the first run [Fig. 3(a)]. The maximum intensity of V_{VCM} appears at approximately 5.6–7.2 GPa, similar to the behavior in the second run [Fig. 4(a)]. The highest Curie temperature appeared at approximately 11.2–14.2 GPa. The values are consistent with those of the Néel temperatures in the dhcp structure, reported in the previous electrical resistance measurement [15]. The FM signal at $P = 21.1$ GPa was suppressed to one-twentieth of that at 7.2 GPa. The results below 10 K are as follows. As seen in Fig. 6(a), the superconducting shielding signal due to Pb shifted toward the low T side with increasing P, and appeared at approximately 2 K and 21.1 GPa. At $P = 21.1$ GPa, a new diamagnetic signal like superconducting shielding signal appeared at approximately 5 K. At 24.8–30.8 GPa, the signal consistently appeared at

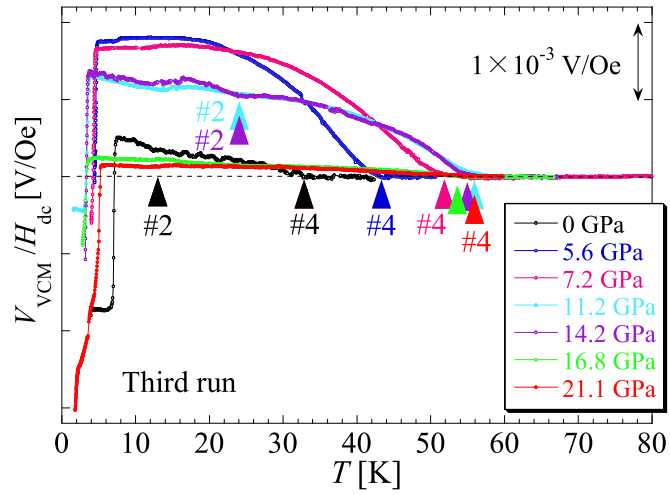

FIG. 5. T-dependence of V_{VCM}/H_{dc} for the third run, covering the P range to 21.1 GPa (at maximum 30.8 GPa), below which the structure changes as Sm-type → dhcp → fcc → distorted fcc. The H_{dc} value is 30 Oe except for 24 Oe at 0 GPa.

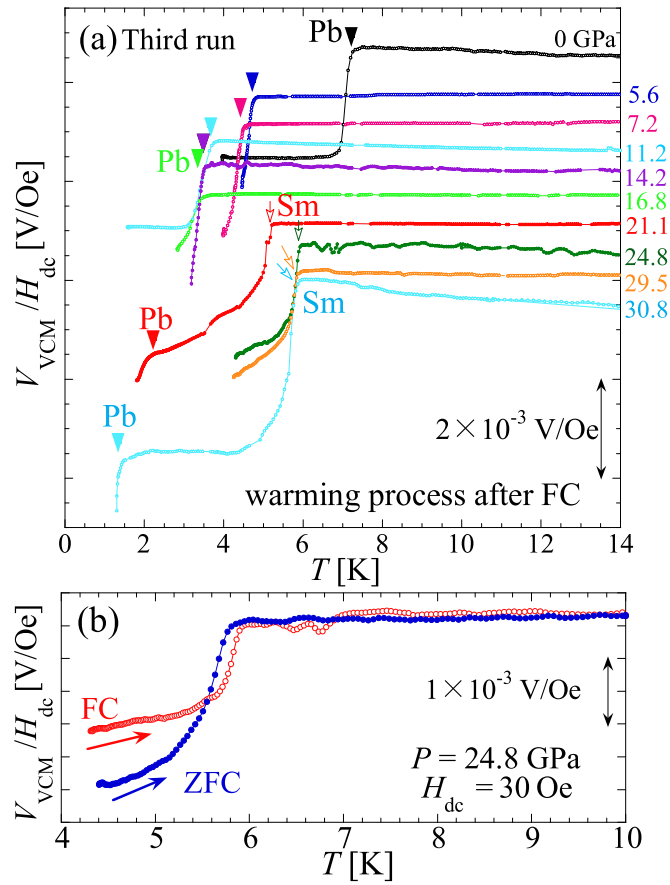

FIG. 6. T-dependence of V_{VCM}/H_{dc} for the third run up to 30.8 GPa. The H_{dc} value is 30 Oe except for 24 Oe at 0 GPa. The low-T data in Fig. 5 are enlarged in (a) with addition of the data for $P >$ 21.1 GPa. (b) For 24.8 GPa, there are two data points in the warming processes after ZFC and FC at $H_{dc} = 30$ Oe.

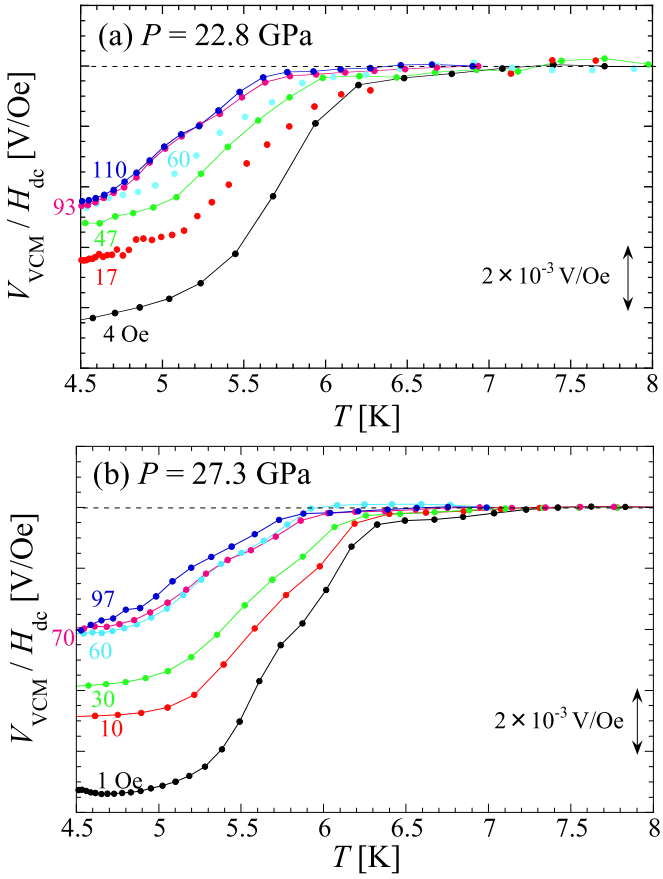

FIG. 7. T-dependence of V_{VCM} for Sm in the fourth run. V_{VCM} proportional to the magnetization is normalized with the applied dc magnetic field H_{dc}. H_{dc} was increased up to 110 Oe. In the fourth run, the pressure was focused to $P = 22.8$ and 27.3 GPa, corresponding to the pressure range of the distorted fcc structures.

approximately 6 K. As seen in Fig. 6(b), the diamagnetic signal after FC is smaller than that after ZFC.

B. H_{dc}-dependence of V_{VCM} in the distorted fcc structure

To investigate the physical property of the diamagnetic signal appearing in the distorted fcc structure, we performed the SQUID-VCM measurements at several H_{dc}'s. Figure 7 shows the T-dependence of V_{VCM} for Sm in the fourth run for $P = 22.8$ [Fig. 7(a)] and 27.3 GPa [Fig. 7(b)]. Figure 8 shows the H_{dc} dependence of offset temperature T_{sc} observed in the fourth run.

Below let us discuss the origin of the diamagnetic signal observed in the distorted fcc structure: Given the following experimental facts, we can assume the appearance of superconductivity as a promising possibility: (1) The diamagnetic signal appeared after the ferromagnetic signal was sufficiently suppressed. (2) This phenomenon was observed consistently in the same P and T regions over three (the second, third, and fourth) runs changing the sample as well as gasket. (3) These attractive signals have never been observed in the other experiments using the same DAC and the same kind of gasket [19,24].

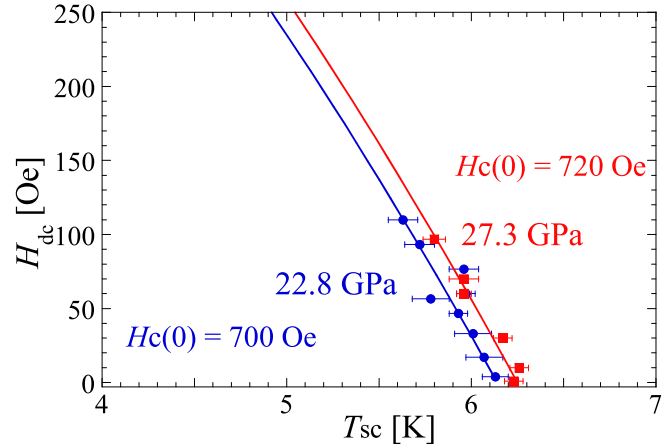

FIG. 8. H_{dc} dependence of offset temperature T_{sc} at $P = 22.8$ GPa and 27.3 GPa in the fourth run. Solid curves represent $H_{\mathrm{dc}} = H_{\mathrm{c}}(0)\{1 - [T/T_{\mathrm{sc}}(0)]^2\}$ with $T_{\mathrm{sc}}(0) = 6.14$ (blue) and 6.25 K (red).

If the diamagnetic signal would originate from superconductivity, we could do the fitting for the H_{dc} dependence of T_{sc}. Given both $H_{\mathrm{c}}(0)$ as critical field at zero temperature and $T_{\mathrm{sc}}(0)$ as T_{sc} at zero field, experimental results are reproduced with $H_{\mathrm{dc}} = H_{\mathrm{c}}(0)\{1 - [T/T_{\mathrm{sc}}(0)]^2\}$. At $P = 22.8$ GPa, $H_{\mathrm{c}}(0) = 700$ Oe and $T_{\mathrm{sc}}(0) = 6.14$ K, and at $P = 27.3$ GPa, $H_{\mathrm{c}}(0) = 720$ Oe and $T_{\mathrm{sc}}(0) = 6.25$ K.

IV. DISCUSSION

Figure 9 shows the P-T phase diagram, which presents information on the V_{VCM} intensity and crystal structure. The critical T determined via R measurements [15] is also plotted and traces the T below which V_{VCM} begins to increase. The trend in the shifting of #4 reveals the transformation from multistepwise AFM state to single FM one, and that of #2 leads to the R anomalies observed at above 35 GPa as seen in Fig. 1(b). At the phase boundary between the Sm-type and dhcp phases, the FM state (ferrimagnetic or weak-FM) is stabilized. At the phase boundary between the dhcp and fcc phases, the FM state is highly unstable. Even after the transformation to the distorted fcc phase, V_{VCM} is not perfectly zero. There, if the diamagnetic signal suggests the existence of superconducting state, the magnetic and superconducting states may coexist, and the superconducting state is stabilized at below 5–6 K.

In the third run, the volume ratio of Pb against Sm in the sample chamber is approximately 15 : 85. The ratio of the diamagnetic signal of Sm against that of Pb is roughly twice. If the diamagnetic signal originates from the superconductivity, the volume fraction of superconducting shielding for Sm is roughly estimated to be 40%. Pb exhibits relatively sharp superconducting signal even at high pressure above 10 GPa, and the magnitude of its superconducting signal does not change largely. Ordinary superconductors, however, exhibit the decrease in superconducting shielding under pressure, because dislocations and defects by structural distortion results in a reduction in the crystallite size. Considering the above situation, if we would have found out the superconductivity,

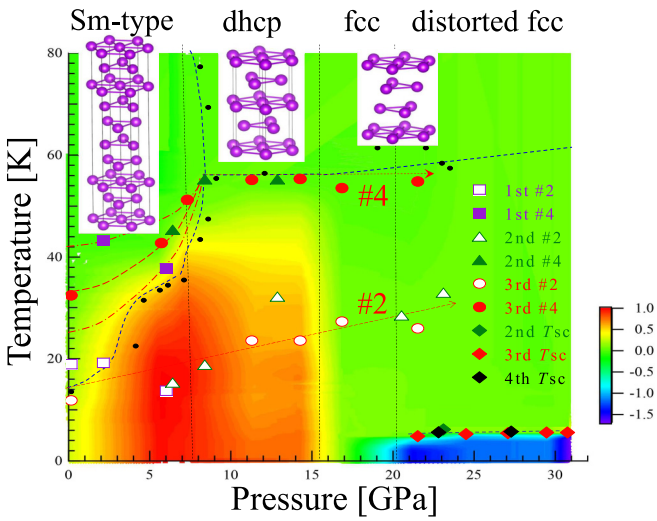

FIG. 9. *P-T* phase diagram determined by the present experiments. Previous results published in the literature on the *R* measurements [15] are plotted with solid black circles. The characteristic temperatures #2 and #4, determined via three runs, are plotted with open and closed symbols, respectively. The trends in the shifting of #2 and #4 are presented with red broken curve and dotted line. The offset temperatures, likely suggesting superconducting transition temperature, determined via three runs are plotted with solid diamonds. The intensity of V_{VCM} is represented by colors ranging from red (positive) to blue (negative). The red region denotes the FM state, while the blue region denotes the diamagnetic state.

we could consider that superconducting volume fraction of Sm for $P > 30$ GPa is much larger than 40%.

The reliable *R* measurements at pressures up to 43 GPa [14] (rolled thin specimen with 99.9% purity), 47 GPa [15] (no description about specimen), and 150 GPa [16] (prepared from ingot) were recently conducted without using a pressure transmitting medium. The first and the third experiments were performed at low temperatures down to liquid ^{4}He temperature [16], whereas no signal due to the superconductivity was observed. To verify whether the appearance of superconductivity is related with both the existence of the pressure transmitting medium and its quality or not, the *R* measurements must be performed in the same hydrostatic condition to that in the present SQUID-VCM experiment. Furthermore, as a possibility, the appearance of the diamagnetic signal migh be related with the existence of residual strain in the prepared sample. In the future, the electronic state calculations as well as neutron diffraction experiment would be also desired.

V. CONCLUSION

To the best of our knowledge, the present experiment is the first successful magnetic measurement of Sm under pressure. The high sensitivity and high accuracy of the SQUID-VCM enabled us to detect the magnetic signal of Sm at high pressure in the GPa range. The study revealed the change in the magnetic states, as individual AFM states at two kinds of atomic cites in the Sm-type phase → ferrimagnet or a weak-ferromagnet in the area near the phase boundary between the Sm-type and dhcp phases → small magnetization state in the fcc phase → the diamagnetic state in the distorted fcc phase. The magnetic field dependence suggests that the diamagnetic signal might be related with the appearance of superconductivity.

ACKNOWLEDGMENTS

This work was supported by JSPS KAKENHI Grants No. JP17H03379 and No. JP19KK0070.

[1] M. Debessai, T. Matsuoka, J. J. Hamlin, J. S. Schilling, and K. Shimizu, Phys. Rev. Lett. **102**, 197002 (2009).
[2] M. Ruderman and C. Kittel, Phys. Rev. **96**, 99 (1954).
[3] T. Kasuya, Prog. Theor. Phys. **16**, 45 (1956).
[4] K. Yosida, Phys. Rev. **106**, 893 (1957).
[5] J. S. Olsen, S. Steenstrup, L. Gerward, U. Benedict, J. Akella, and G. Smith, High Pressure Res. **4**, 366 (1990).
[6] R. Husband, I. Loa, K. Munro, and M. McMahon, J. Phys.: Conf. Ser. **500**, 032009 (2014).
[7] M. Mito, Y. Kimura, K. Yamakata, M. Ohkuma, H. Chayamichi, T. Tajiri, H. Deguchi, and M. Ishizuka, Phys. Rev. B **103**, 024444 (2021).
[8] W. C. Koehler and R. M. Moon, Phys. Rev. Lett. **29**, 1468 (1972).
[9] S. Lee, E. Forgan, S. Shaikh, C. Tang, W. Stirling, S. Langridge, A. Rollason, M. Costa, M. Cooper, E. Zukowski *et al.*, J. Magn. Magn. Mater. **127**, 145 (1993).
[10] S. Arajs and G. R. Dunmyre, Z. Naturforsch **21**, 1856 (1955).
[11] L. D. Jennings, E. D. Hill, and F. H. Spedding, J. Chem. Phys. **31**, 1240 (1959).
[12] P. Wachteri, in *Handbook on the Physics and Chemistry of Rare Earths*, Vol. 19, edited by K. A. Gschneidner *et al.* (North-Holland, Amsterdam, 1994), p. 383.
[13] A. Barla, J.-P. Sanchez, J. Derr, B. Salce, G. Lapertot, J. Flouquet, B. P. Doyle, O. Leupold, R. Ruffer, M. M. Abd-Elmeguid *et al.*, J. Phys.: Condens. Matter **17**, S837 (2005).
[14] W. Y. Dong, T. H. Lin, K. J. Dunn, and C. N. J. Wagner, Phys. Rev. B **35**, 966 (1987).
[15] C. R. Johnson, G. M. Tsoi, and Y. K. Vohra, J. Phys.: Condens. Matter **29**, 065801 (2017).
[16] Y. Deng and J. S. Schilling, Phys. Rev. B **99**, 085137 (2019).
[17] M. Mito, K. Matsumoto, Y. Komorida, H. Deguchi, S. Takagi, T. Tajiri, T. Iwamoto, T. Kawae, M. Tokita, and K. Takeda, J. Phys. Chem. Solid **70**, 1290 (2009).
[18] M. Ishizuka, Rev. Sci. Instrum. **76**, 123902 (2005).

[19] M. Abdel-Hafiez, M. Mito, K. Shibayama, S. Takagi, M. Ishizuka, A. N. Vasiliev, C. Krellner, and H. K. Mao, Phys. Rev. B **98**, 094504 (2018).

[20] K. Murata, H. Yoshino, H. O. Yadav, Y. Honda, and N. Shirakawa, Rev. Sci. Instrum. **68**, 2490 (1997).

[21] G. J. Piermarini, S. Block, J. D. Barnett, and R. A. Forman, J. Appl. Phys. **46**, 2774 (1975).

[22] K. Irie, K. Shibayama, M. Mito, S. Takagi, M. Ishizuka, K. Lekin, and R. T. Oakley, Phys. Rev. B **99**, 014417 (2019).

[23] See Supplemental Material at http://link.aps.org/supplemental/10.1103/PhysRevB.104.054431 for more details on this phenomenon.

[24] M. Mito, S. Shigeoka, H. Kondo, N. Noumi, Y. Kitamura, K. Irie, K. Nakamura, S. Takagi, H. Deguchi, T. Tajiri *et al.*, Mater. Trans. **60**, 1472 (2019).